Unexpected plasticization effects on the structure and properties of polyelectrolyte complexed chitosan/alginate materials

Pei Chen [a,b], *Fengwei Xie* [b,c,*,†], *Fengzai Tang* [d], *Tony McNally* [b,**]

[a] College of Food Science, South China Agricultural University, Guangzhou, Guangdong 510642, China

[b] International Institute for Nanocomposites Manufacturing (IINM), WMG, University of Warwick, Coventry CV4 7AL, United Kingdom

[c] School of Chemical Engineering, The University of Queensland, Brisbane, Qld 4072, Australia

[d] WMG, University of Warwick, Coventry CV4 7AL, United Kingdom

Corresponding Authors

* Fengwei Xie. Email: d.xie.2@warwick.ac.uk, fwhsieh@gmail.com

** Tony McNally. Email: t.mcnally@warwick.ac.uk

KEYWORDS*: Polysaccharide; Thermomechanical processing; 1-Ethyl-3-methylimidazolium acetate; Glycerol; Triacetin; Plasticization; Surface hydrophilicity*

ABSTRACT: This work describes the effects of different plasticizers, namely glycerol, triacetin, and 1-ethyl-3-methylimidazolium acetate ([C_2mim][OAc]), on the structure and properties of thermomechanically-processed, bulk chitosan and chitosan/alginate materials. Mechanical data shows that, for the chitosan matrix, glycerol and [C_2mim][OAc] were highly effective at reducing intra- and intermolecular forces between biopolymer chains, leading to increased ductility, while the plasticization effect of triacetin was minor. Nonetheless, this triester effectively suppressed biopolymer re-crystallization whereas [C_2mim][OAc] promoted it. In contrast, for the chitosan/alginate matrix, inclusion of triacetin resulted in more re-crystallization, higher thermal stability, and excellent mechanical properties. The triacetin assisted the interactions between biopolymer chains in this polyelectrolyte complexed system. In contrast, the chitosan/alginate material plasticized by [C_2mim][OAc] displayed the most apparent phase separation, weakest mechanical properties, and highest surface hydrophilicity, behavior associated with the disruption of polyelectrolyte complexation and hydrogen bonding between biopolymer chains. Interestingly, the formation of a "new structure" under the electron beam during microscopy imaging was observed, likely from coordination between alginate and [C_2mim][OAc]. Thus, this work has revealed the strong and unexpected effects of three different plasticizers on the hydrogen bonding and electrostatic interactions within chitosan/alginate polyelectrolyte complexed materials, which have potential for biomedical applications where balanced hydrophilicity and mechanical properties are required.

INTRODUCTION

Biopolymers (*e.g.*, cellulose, chitin/chitosan, alginate, starch, and proteins) are a class of polymers that can be directly sourced from nature and are renewable. Critically, they are low/non-toxic, biodegradable, biocompatible, and inherently functional. Moreover, they have high chemical versatility due to abundant reactive groups on the backbone chain. Therefore, biopolymers have also been widely studied for various biomedical and pharmaceutical applications.[1-6]

Whatever the application, biopolymers need to be processed into certain forms and shapes prior to use. However, biopolymers are synthesized in plants and animals with unique chain interactions and supramolecular structures, which makes them recalcitrant to dissolution and plasticization. For the disruption of the original hydrogen-bonded network, a suitable solvent, which can effectively interact with the biopolymer hydroxyl groups, combined with heat treatment, is usually required. During thermomechanical processing where intensive shear forces are involved, much less solvent (or plasticizer) may be required to disrupt intrinsic hydrogen bonding in and between biopolymers. In this way, plasticized biopolymers could be obtained.[7-8]. The incorporation of plasticizers into biopolymers may also improve processability and properties (*e.g.*, mechanical, moisture and gas barrier, electrical, and thermal), which has been widely studied.[9-10]

In this work, we compare the different plasticization effects of glycerol, 1-ethyl-3-methylimidazolium acetate ([C_2mim][OAc]), and triacetin on the structure and properties of thermomechanically processed chitosan and chitosan/alginate materials. Creating blends or composites based on biopolymers is a simple and cost-effective method to realize new materials with enhanced properties and/or new functionality.[11-14] The electrostatic attraction between the chitosan polycation and the alginate polyanion may lead to polyelectrolyte complexation (PEC).

Recent research demonstrated the advantages of PEC for the development of advanced biopolymer materials with superior properties that single biopolymers cannot achieve, *e.g.* mechanical properties,[15-17] barrier properties,[18] hydrolytic stability,[19] and cell adhesiveness.[20] In polyelectrolyte complexed systems, ionic interactions may lead to the formation of particular structures and complement other interactions (*e.g.* hydrogen bonding). However, the preparation of bulk polyelectrolyte complexed materials is still challenging since rapid complexation between two polymers at the contact interface result in heterogeneous aggregates.[21] Also, how PEC and the structure and properties of complexed biopolymer materials are affected by plasticizers remains largely unknown.

With different chemical polarity and hydrophilicity/hydrophobicity, glycerol and triacetin should have different degrees of interactions with biopolymers. Meanwhile, the groups with different degrees of polarity on biopolymer chains will interact with the plasticizers to different extents, possibly leading to a phase-separated structure.[22] Besides, [C_2mim][OAc], as an ionic liquid (IL) containing a strongly basic, hydrogen-bond-accepting anion (*i.e.*, carboxylate), can disrupt intra- and intermolecular hydrogen bonding in biopolymers.[23] Our hypothesis is that these plasticizers have very different ways of interacting with biopolymers and their effects are highly dependent on matrix type (chitosan or chitosan/alginate). We also propose that triacetin can interact in an unconventional manner with biopolymers to cause structural changes. Our motivation for this work is to understand the phase interactions resulting from the use of different plasticizers, providing options to tailor biopolymer material properties such as surface wettability and mechanical properties, which can better meet the needs of biomedical and pharmaceutical applications.

EXPERIMENTAL SECTION

Materials. Chitosan (poly(β-(1,4)-D-glucosamine), derived from crustaceous shells, with a viscosity of about 200 mPa·s (*i.e.*, 1% solution in 1% acetic acid at 20 °C), and a degree of deacetylation of ≥85%, was purchased from Jinan Haidebei Marine Bioengineering Co., Ltd. (China). The molecular mass of this chitosan is about 250 kDa. Alginate sodium (viscosity: 200±20 mPa·s; M/G ratio: 1:1) was purchased from Shanghai Macklin Biochemical Co., Ltd. (China). Glycerol (≥99% analytical grade) was supplied by Fisher Scientific UK Ltd.; [C_2mim][OAc] (≥95.0%) and triacetin (99%) by Sigma-Aldrich Company Ltd. (UK); formic acid (98% w/w AR) and NaBr (pure) by Scientific Laboratory Supplies Ltd. (UK). Deionized water was used for all experiments.

Sample preparation. Table 1 shows the formulations and codes of the different samples prepared in this work. In these codes, "X" means the matrix was chitosan alone while "Y" indicates chitosan/alginate was the matrix. The following letter indicates the plasticizer used, namely, "G" for glycerol, "E" for [C_2mim][OAc], and "T" for triacetin. The samples were prepared by pre-blending with 2M formic acid solution, thermomechanical kneading at 80°C for 15 min, hot-pressing at 110 °C and 160 bar for 10 min, and conditioning at 57% relative humidity for 3 weeks, as described previously.[19] One of the plasticizers (glycerol, [C_2mim][OAc], and triacetin) was added during pre-blending. After conditioning, the samples were left openly at room temperature (RT) for 5 days before characterization.

Table 1. Sample codes and compositions (represented as portions by weight).

Sample	Chitosan	Alginate	Plasticizer	2M Formic acid
X-F	100	–	–	260.67

XG-F	100	–	20, Glycerol	260.67
XE-F	100	–	20, [C_2mim][OAc]	260.67
XT-F	100		20, Triacetin	260.67
Y-F	50	50	–	260.67
YG-F	50	50	20, Glycerol	260.67
YE-F	50	50	20, [C_2mim][OAc]	260.67
YT-F	50	50	20, Triacetin	260.67

Material characterization. Scanning electron microscopy (SEM) imaging was performed using a Zeiss Sigma field-emission scanning electron microscope with an acceleration voltage of 6 kV. The biopolymer films were cryo-fractured using liquid nitrogen and the samples sputter-coated with gold/palladium before imaging.

Scanning transmission electron microscopy (STEM) was conducted using a Talos F200X transmission electron microscope at 200 kV to obtain both bright-field (BF) and high-angle annular dark-field (HAADF) images. Ribbons of about 60 nm thick were sectioned from epoxy-embedded sample blocks and subsequently transferred onto holey carbon films on 200-mesh copper grids. No liquids were used during sample preparation, to avoid damage to the samples.

Fourier-transform infrared (FTIR) spectra were collected using a Bruker Tensor 27 FTIR spectrometer with an attenuated total reflection (ATR) accessory acquiring 32 scans for each sample over the range 4000–500 cm^{-1} at RT.

X-ray diffraction (XRD) patterns were acquired using a Panalytical Empyrean X-ray diffractometer at 40 kV and 40 mA with a Co target (Kα = 1.790307 Å) and a beam slit of 10 mm. The samples were scanned over an angular range (2θ) of 6–40° with a step size of 0.0263° and a step rate of 2.16 s/step.

Thermo-gravimetric analysis (TGA) was undertaken using a Mettler Toledo TGA apparatus over a temperature range of 30–700 °C at 10 K/min under nitrogen.

Dynamic mechanical thermal analysis (DMTA) was performed using a Tritec 2000 DMA (Triton Technology Ltd., UK) in dual cantilever mode with a sample length of 5 mm at a displacement of 0.01 mm. Temperature scans were performed from −100 °C to 180 °C at 2 °K/min and 1 Hz.

Tensile testing was performed using an Instron 3367 universal testing machine with a 1kN load cell at a crosshead speed of 3 mm/min. As the specimens were in the form of thin sheets, specimen extension was measured by grip separation as suggested by ASTM Standard D882. At least seven replicates were used for each sample.

Contact angle (θ_c) data was obtained from sessile tests at RT based on Young–Laplace using an Attension Theta Lite instrument (Biolin Scientific, UK). As θ_c kept changing after a drop of water was placed onto the sample surface, θ_c values at 0 s, 30 s, and 60 s (denoted as θ_{c0s}, θ_{c30s}, and θ_{c60s} respectively) were recorded.

Electrical impedance spectroscopy (EIS) was performed using a Princeton Applied Research PARSTAT MC (PMC) multi-channel potentiostat (Ametek Scientific Instruments, USA) with a PMC-2000 card and a two-point probe. The two surfaces of samples were painted with carbon conductive grease (No.8481, MG Chemicals, Canada) in designated areas (24 × 24 mm). Each sample was measured in triplicate. The real (Z') and imaginary (Z'') parts of impedance were acquired within a frequency (f) range of 1–10^6 Hz. The AC conductivity (admittance) (σ), the real part of relative permittivity (ε'_r), and the imaginary part of electric modulus (M'') were calculated using the following equations:[24-26]

$$\sigma = \frac{Z'}{Z'^2 + Z''^2} \cdot \frac{t}{A} \quad (1)$$

$$\varepsilon'_r = \frac{-Z''}{Z'^2 + Z''^2} \cdot \frac{t}{\omega A \varepsilon_0} \quad (2)$$

$$M'' = \frac{\varepsilon''}{\varepsilon'^2 + \varepsilon''^2} \quad (3)$$

where, ω is the angular frequency (= $2\pi f$), ε_0 is the permittivity of free space (≈ 8.854 $\times 10^{-12}$ F·m^{-1}), A is the tested area of the sample (m^2), and t is the sample thickness (m).

The bulk resistance (R_b) was determined from the Nyquist plots of impedance (Z'' *vs.* Z') from the points where the semicircle and the straight line meet. Then, the conductivity (σ_{dc}) can be calculated using equation (4):[24, 27]

$$\sigma_{dc} = \frac{t}{R_b \cdot A} \quad (4)$$

RESULTS AND DISCUSSION

Morphology. SEM images (**Figures S1**) show that unprocessed chitosan and alginate have an un-compacted structure with crevices. In comparison, all the chitosan (X) films showed a cohesive and firm structure, indicating successful processing of the biopolymers. In particular, both X-F and XE-F exhibited a very smooth fractured surface. For XT-F, there were some cavities and protrusions with sizes up to about 1 μm on the surface. This feature could be triacetin-concentrated domains. Due to its hydrophobicity, triacetin may have weak interaction with chitosan.[28]

Compared with the X-series, the Y-series presented less smooth surfaces. The least cohesive structure was displayed by YE-F. For this sample, while there are strong interactions between the $[OAc]^-$ anion and the hydroxyl and amine groups of chitosan, the $[C_2mim]^+$ cation may bind with the carboxylate groups of alginate due to the reverse charges, which might account for the highest degree of phase separation in YE-F and possibly weakened PEC. Like XT-F, YT-F also showed cavities and protrusions on the surface, which could reflect triacetin-rich domains.

The morphology of the different samples was further examined using STEM, as shown in **Figure 1**. The X-series, in general, displayed a homogeneous microstructure (The band and line features in the low-magnification images for the X-series samples were induced from microtoming the samples). In contrast, for the Y-series, a second phase (rich in alginate, the brighter areas in the STEM-HAADF images) distinct from the chitosan-rich phase can be observed, corresponding to the inhomogeneity seen when examined by SEM. Thus, while both chitosan and alginate contain hydrophilic groups (*i.e.*, hydroxyl, amine, or carboxyl), they are not fully compatible probably caused by their thermodynamic difference (*e.g.*, different ways of chain aggregation such as the helical conformation of alginate).

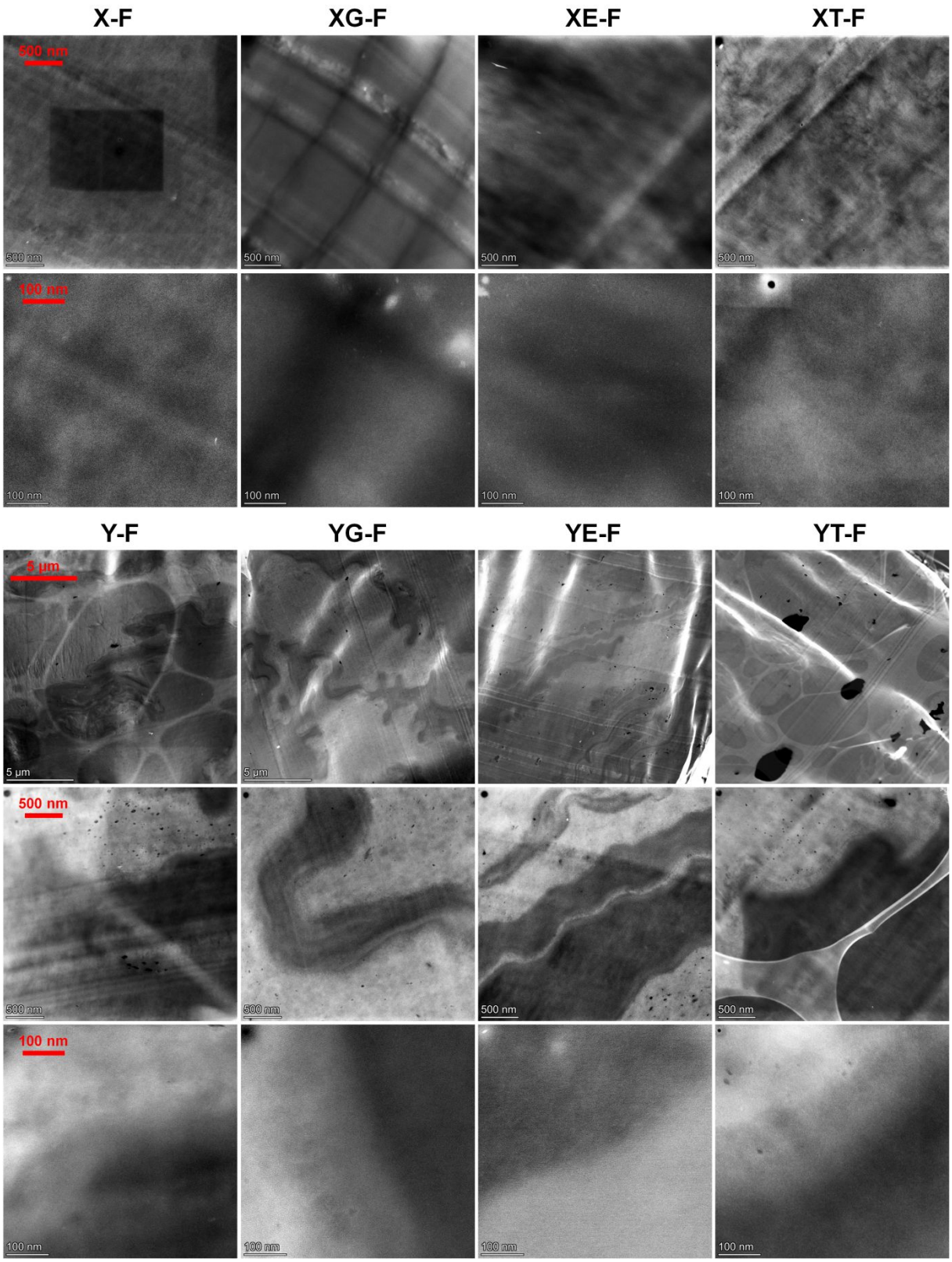

Figure 1. STEM-HAADF images of the different biopolymer films.

Only for YE-F, during the STEM imaging, we surprisingly observed the generation of a "new structure" normally in the edges of imaged areas (where the material has no or much less interaction with the electron beam) (see **Figure S2**). It looks like that some material migrated into the areas adjacent to the region imaged driven by the electron beam; as such, the initial equilibrium at the areas outside of this region is broken, giving rise to the generation of the "new structure". Nonetheless, the "new structure" was unstable and became difficult to observe rapidly (within a few seconds) when directly exposed under the electron beam, as shown in **Video Clip S1** (STEM-HAADF) and **Video Clip S2** (STEM-HAADF). The "new structure" appears as scattered spots or as a helical shape. Previous research[29-31] suggested that alginate chains tend to form helical structures through intramolecular hydrogen bonding and coordinate with Ca^{2+} to form junction zones. We speculate that the energy from the electron beam may facilitate the coordination between alginate and $[C_2mim]^+$ and the packing of biopolymer chains to form a new structure (possibly crystals). This interesting phenomenon is worth further investigation.

Molecular interactions. Figure 2 shows the FTIR spectra for the different samples. The X-series of biopolymer films displayed FTIR patterns very similar to each other but quite different from that of unprocessed chitosan. Specifically, a prominent peak emerged at 1570 cm^{-1} (N─H bending) with a shoulder at 1530 cm^{-1} (partial protonation of the amine group of chitosan, *i.e.*, ─$NH3^+$).[32] The characteristic peak originally at 1265 cm^{-1} (Amide III) red shifted and the one at 1059 cm^{-1} (asymmetric C─O─C stretching in the glycosidic linkage)[32-34] blue shifted. Therefore, it is likely that the hydrogen bonding in the processed chitosan films mainly involved amine and amide groups and also affected the polysaccharide backbone.

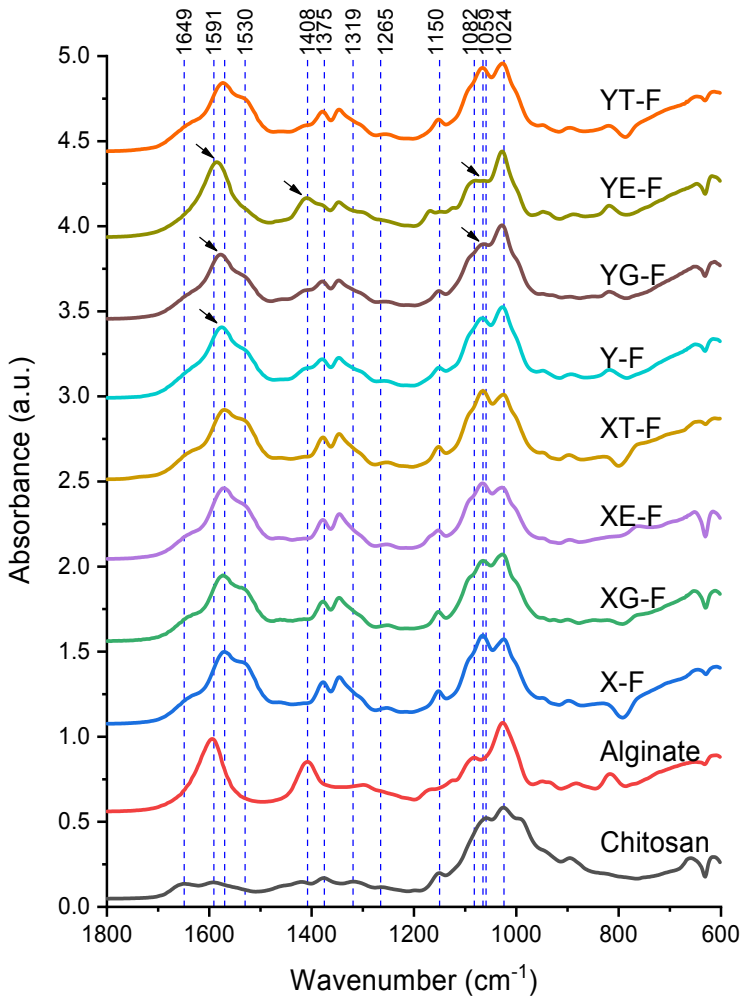

Figure 2. FTIR spectra for chitosan, alginate, and the different biopolymer films. The reference lines indicate characteristic bands for unprocessed alginate (1591 cm^{-1}, 1408 cm^{-1}, 1300 cm^{-1}, 1082 cm^{-1}, and 1024 cm^{-1}) and chitosan (1649 cm^{-1}, 1591 cm^{-1}, 1420 cm^{-1}, 1375 cm^{-1}, 1319 cm^{-1}, 1265 cm^{-1}, 1150 cm^{-1}, 1059 cm^{-1}, and 1024 cm^{-1}). The arrows indicate shifts in peak position or changes in peak intensity.

The Y-samples displayed FTIR spectra similar to those for the X-series, with additional peaks at 1408 cm^{-1} (symmetric COO^- stretching), 1300 cm^{-1} (skeletal vibration of C─CH and O─CH bending), and 1082 cm^{-1} (asymmetric C─O─C stretching in the glycosidic linkage), which are

characteristic of alginate.[32, 35] Some differences in the FTIR spectra among the Y-samples can be noticed. While YT-F showed the peak at 1570 cm^{-1} as for the X-series without any shift, this peak appeared at higher wavenumbers for Y-F, YG-F, and YE-F. Furthermore, for YE-F, the shoulder at 1530 cm^{-1} (─$NH3^{+}$) and the peak at 1059 cm^{-1} became much weaker, and the peak at 1408 cm^{-1} (symmetric COO^{-} stretching) stronger, *i.e.*, the FTIR spectrum for YE-F exhibited more features of alginate. This indicates that inclusion of [C_2mim][OAc] resulted in weak interactions between chitosan and alginate. Glycerol may have also weakened the interaction between chitosan and alginate but not to the same extent as the IL.

Crystalline structure. Figure 3 shows the XRD curves for the different samples. All the X-samples had similar XRD patterns, which were different from that for unprocessed chitosan. These films displayed three major peaks at 2θ = 13.5° ((020) reflection, *d*-spacing = 0.76 nm), 21.7° ((100) reflection, 0.48 nm), and 27.2° ((110) reflection, 0.38 nm), which are all attributed to the crystal lattice of chitosan.[36] The shift of the (100) reflection from 23.3° to 21.7° 2θ indicates an enlarged *d*-spacing of the chitosan crystal lattice. Also, there were some small peaks at 2θ = 10.0° (1.03 nm), 19.0° (0.54 nm), and 30.8° (0.34 nm). As the XRD pattern of processed chitosan was different from that of original chitosan, processing almost fully destroyed the original crystalline structure and, subsequently, new biopolymer crystals were formed.

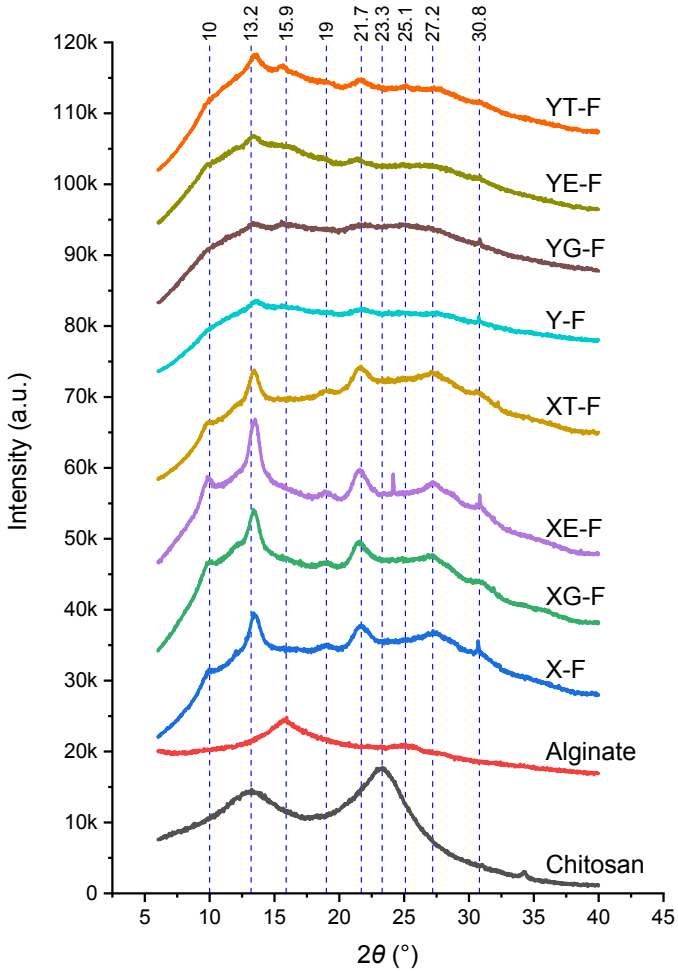

Figure 3. XRD patterns for chitosan, alginate, and the different biopolymer films. The reference lines indicate characteristic peaks for unprocessed chitosan (13.2° and 23.3°), unprocessed alginate (15.9° and 25.1°), and X-F (10°, 19°, 21.7°, 27.2°, and 30.8°).

Compared with X-F, XE-F displayed apparently more-intense XRD peaks while XT-F had less-intense peaks (especially at 13.5° 2θ). Given this, [C_2mim][OAc] may have assisted the re-crystallization of the biopolymer whereas triacetin hindered it.

The Y-samples displayed XRD peaks similar to those for the X-series along with the two characteristic reflections of alginate, but all having weak intensities. Among the Y-series, YT-F

had the strongest reflections followed by YE-F, whereas Y-F and YG-F were mostly amorphous. Processing had largely destroyed the original crystalline structures of chitosan and alginate and interactions (PEC and hydrogen bonding) between the two biopolymers constrained their re-crystallization. Compared with Y-F and YG-F, YE-F was more crystalline, which could result from its greater degree of phase separation and lower degree of PEC. The highest crystallinity among the Y-series was shown by YT-F, suggesting that triacetin assisted the re-crystallization of both biopolymers.

Thermal stability. Figure 4 shows the TGA results in the form of derivative weight as a function of temperature. For chitosan, the weight loss occurred between 235 °C and 385 °C, with the peak temperature being 289 °C (T_d, with the maximum weight loss rate). For X-F, a small peak evolved between 205 °C and 245 °C, likely due to the initial de-polymerization of chitosan. X-F had T_d = 297 °C and XT-F had T_d = 291°C, both higher than that of unprocessed chitosan. The enhanced thermal stability is probably due to the more ordered structure and/or a higher degree of the hydrogen-bonding resulting from the processing. In contrast, XG-F and XE-F displayed lower thermal stability (T_d = 283 °C and 264 °C, respectively). Both glycerol[37] and [C_2mim][OAc][38] have lower thermal stability, which could make the plasticized chitosan more thermally sensitive. Specifically, the earlier thermal decomposition of the plasticizer could generate free radicals, which could accelerate biopolymer chain scission with increasing temperature.

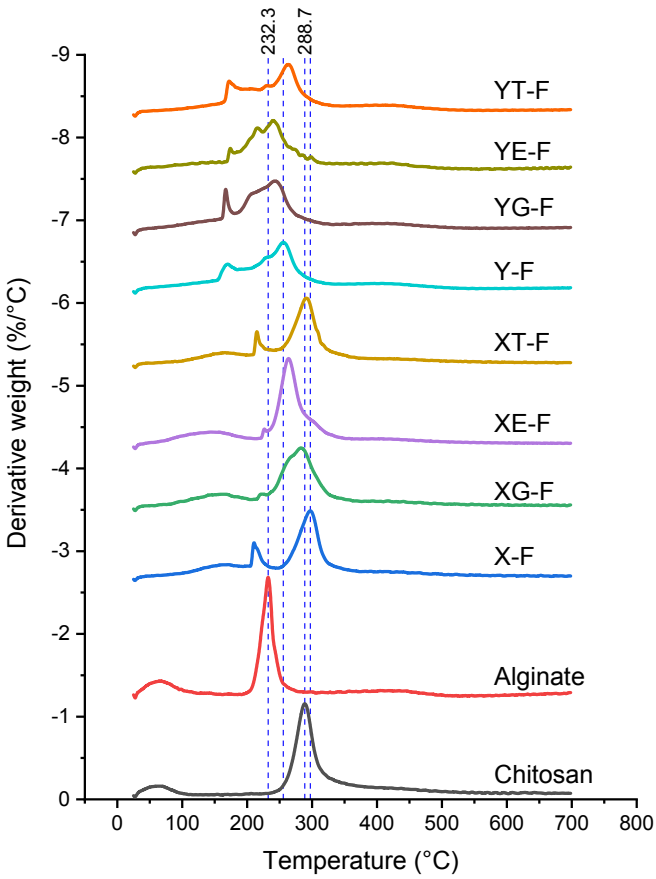

Figure 4. Derivative-weight-loss curves for chitosan, alginate and the different biopolymer films. The reference lines indicate the peak thermal decomposition temperatures of unprocessed chitosan (288.7 °C), unprocessed alginate (232.7 °C), X-F (297.2 °C), and Y-F (255.7 °C).

For Y-F, the weight loss mainly occurred between 154 °C and 330 °C with T_d = 256 °C. Given this, the incorporation of alginate in the chitosan matrix led to substantially reduced thermal stability. This is caused by the inherent low thermal stability of alginate (weight loss range 195–280 °C, T_d = 289 °C), possibly due to its carboxyl group, which is thermally labile. Compared with Y-F, YT-F displayed obviously higher T_d (263 °C). This enhanced thermal stability might be due to its higher crystallinity as determined from XRD. In contrast, plasticization by glycerol or

[C_2mim][OAc] led to reduced thermal stability (T_d = 243 °C for YG-F and 240 °C for YE-F). Moreover, for Y-F and YT-F, the peak for alginate at 232 °C was still visible but small. This could indicate there were interactions between chitosan and alginate despite some degree of phase separation (as discussed in STEM). In comparison, for both YG-F and YE-F, this peak originally at 232 °C appeared at a lower temperature and became more pronounced, indicating less interactions and a lower degree of compatibility between the two biopolymers.

Molecular relaxations. DMTA (**Figure 5**) indicates that all the biopolymer films displayed two loss tangent (tan δ) transitions, a weak transition below 0 °C associated with the motions of the side chains or lateral groups of chitosan (β-relaxation). And, above RT, a much more prominent transition, which is attributed to the α-transition (glass transition) of chitosan.[39-40] Overall, for both X- and Y-matrices, the intensities and locations of the two transitions were largely influenced by plasticizer type.

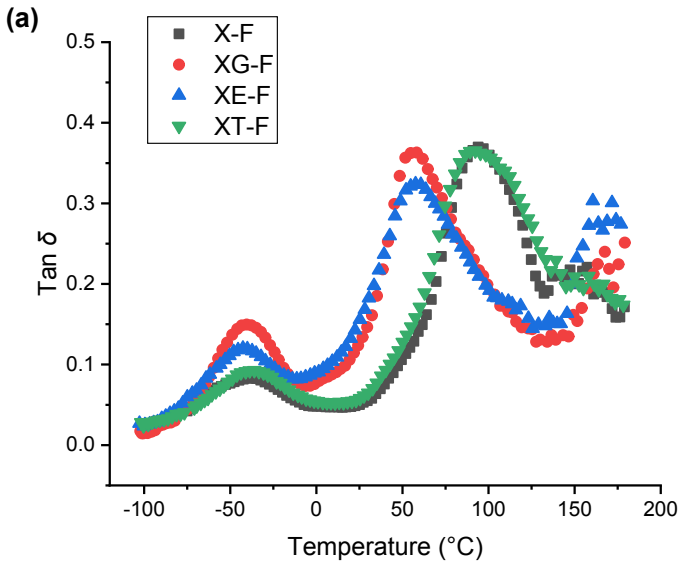

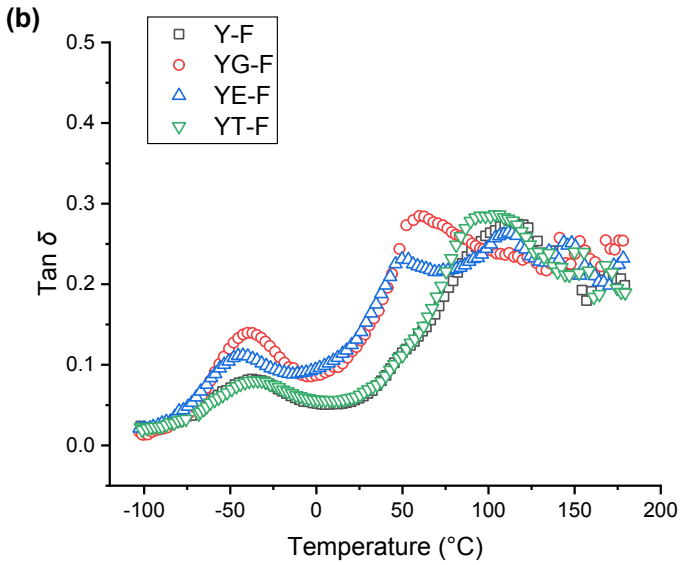

Figure 5. Loss tangent (tan δ) as a function of temperature for the different biopolymer films: a) chitosan matrix and b) chitosan/alginate matrix.

For X-F, the peak temperature of the β-transition (T_β) was −38 °C and that of the α-transition (T_α) was 95 °C. In comparison, XG-F displayed a more intense β-transition with T_β = −41 °C, likely due to the interaction of glycerol with the side chains or lateral groups of chitosan. Furthermore, the T_α decreased significantly to 56 °C, indicating inclusion of glycerol made the chitosan chains more mobile. XE-F exhibited similar T_α and T_β values as those for XG-F, although both peaks became less intense. The two transitions observed for XT-F matched those of X-F although T_α was slightly lower (89 °C). A previous study[28] highlighted the weak interactions between triacetin and biopolymers. Subsequently, triacetin may have a limited effect on the mobility of the main chains of chitosan in the amorphous regions.

The incorporation of alginate in the matrix mainly affected the α-transition, which became less intense and less sharp. Y-F had higher T_α than X-F. Compared with XG-F, YG-F had a weak α-transition with similar T_α but tan δ decreased less abruptly after the peak temperature. The

comparison between XT-F and YT-F indicate a similar situation. For Y-F, YG-F, and YT-F, the α-transition peak could be an overlap of the α-transitions for chitosan and alginate respectively, although interactions between the two biopolymers may have restricted chain mobility. Moreover, compared with XE-F, YE-F seemed to have two α-transitions, one with a peak maximum at 49 °C and the other at 111 °C. This could indicate a low degree of compatibility between the two biopolymers, in agreement with the apparent phase separation, see STEM images and thermal stability.

Tensile mechanical properties. Figure 6 (a) shows representative stress–strain curves for the different biopolymer films, which can be all considered as hard and tough polymers but with different degrees of strain hardening. Generally, the X-series were tougher than the Y-series. For both matrices, the inclusion of triacetin did not increase ductility. XT-F and YT-F were more brittle than X-F and Y-F, respectively. The triacetin-rich domains in the biopolymer matrices (as seen in SEM images) contributed to diminishing mechanical properties.

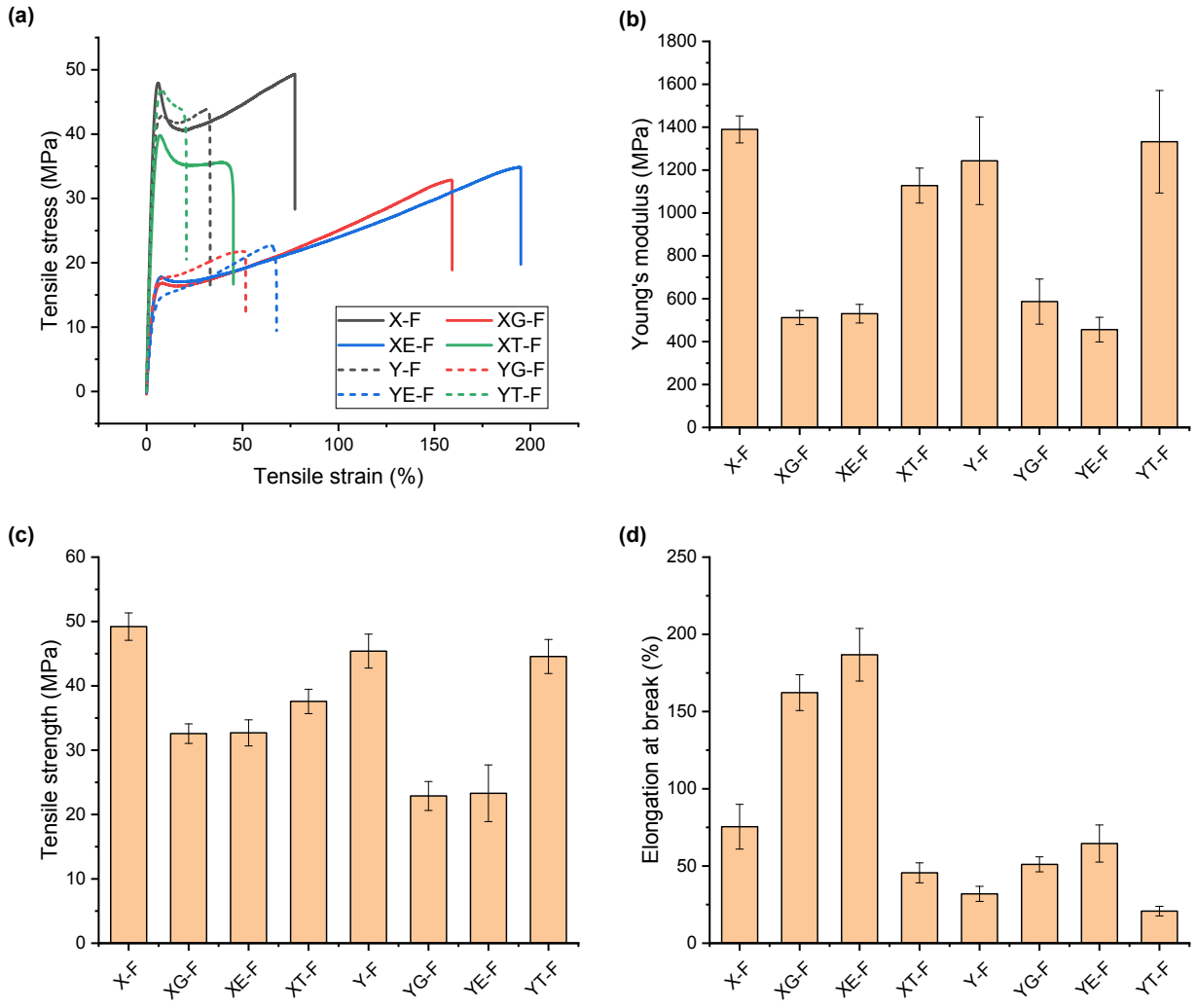

Figure 6. a) Representative stress–strain curves under tensile testing for the different biopolymer films; b) tensile strength; c) Young's modulus; and d) Elongation at break of the different biopolymer films. Error bars represent standard deviations.

Based on the stress–strain curves, Young's modulus (E), tensile strength (σ_t), and elongation at break (ε_b) were determined, see **Figure 6** (b), (c) and (d). Overall, irrespective of matrix, the samples plasticized by glycerol and [C_2mim][OAc] displayed lower E and σ_t but higher ε_b, suggesting greater ductility. This is as expected for the action of a plasticizer, which can reduce

the number of hydrogen bonds and act as a spacer between biopolymer chains. For both matrices, the IL led to moderately higher ε_b than glycerol. Given this, compared with glycerol, the IL should have stronger hydrogen-bonding capability to interact with biopolymers. YE-F had comparable mechanical properties as YG-F, suggesting probably the hydrogen bonds formed during the conditioning played a dominant role in determining mechanical properties. When triacetin was used as a plasticizer, significantly increased E and σ_t and decreased ε_b were achieved. Compared with X-F and Y-F, XT-F and YT-F showed even lower ε_b values with similar or even lower E and σ_t, suggesting the more brittle nature of the triacetin-plasticized samples.

Additionally, the Shore D hardness values for the different samples were also measured, see **Figure S3**. Matrix and plasticizer types influenced hardness and the same trends observed for tensile properties (E and σ_t) were obtained for hardness. The lowest Shore D hardness was displayed by the samples with [C_2mim][OAc] added, which, again, shows the strongest plasticizing effect for these biopolymers. It is proposed that, compared with the other plasticizers, the IL could more effectively increase chain mobility and free volume in the biopolymer(s).

Surface wettability. The contact angle (θ_c) results are shown in **Figure 7**, a measure of the variation in film surface wettability of the different biopolymer films. X-F had θ_{c0s} = 104±3°, θ_{c30s} = 76±4°, and θ_{c0s} = 71±3°. While XG-F displayed similar values as X-F, XE-F had marginally lower θ_{c0s} (95±3°) but similar θ_{c30s} and θ_{c60s}, which could be due to the higher hydrophilicity of [C_2mim][OAc] but the enhanced crystallinity of chitosan. Whilst XT-F had similar θ_{c0s} as X-F, the θ_{c30s} and θ_{c60s} for the former were moderately lower, which might be due to its more amorphous structure (see XRD results).

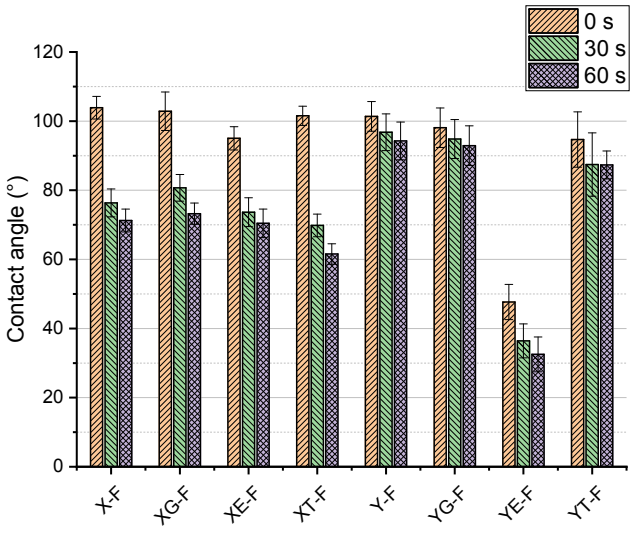

Figure 7. Contact angle values for the different biopolymer films at 0 s, 30 s, and 60 s. Error bars represent standard deviations.

Compared with X-F, Y-F had similar θ_{c0s} (101±4°) but significantly higher θ_{c30s} (97±5°) and θ_{c0s} (94±5°), indicative of its hydrophobic surface ($\theta_c > 90°$). The increased surface hydrophobicity of Y-F could undoubtedly be attributed to interactions (PEC and hydrogen bonding) between the two biopolymers while alginate is hydrophilic because of hydroxyl and carboxyl groups. Inclusion of glycerol (YG-F) did not cause any significant difference in θ_c. YT-F had θ_{c0s} = 95±8°, θ_{c30s} = 87±9°, and θ_{c60s} = 87±4°. The moderately increased surface hydrophilicity of YT-F may be due to the slightly weakened PEC and hydrogen bonding by triacetin. Moreover, YE-F showed dramatically decreased θ_{c0s} (48±5°), θ_{c30s} (36±5°), and θ_{c60s} (33±5°). The much higher surface hydrophilicity of YE-F could be ascribed to not only the high hydrophilicity of [C_2mim][OAc], but also the weakened PEC and greater phase separation, as discussed above.

Electrochemical properties. Figure 8 (a) shows the Nyquist plots of impedance (*Z″ vs. Z′*) for the different samples, based on which, R_b and σ_{dc} values were calculated[41] and listed in **Table S1**.

For the X-series, plasticization led to obviously higher σ_{dc}. Given this, the plasticizers increased the mobility of electrical charges (ions and dipoles) in the processed films. Among the X-samples, the highest σ_{dc} was displayed by XE-T, in which case, [C_2mim][OAc] as a salt might further contribute to the amounts of mobile ions in the system. Y-F exhibited a σ_{dc} value similar to those of XE-F. The predominantly amorphous nature of Y-F could be instrumental in determining its electrical conductivity. Compared with Y-F, both YG-F and YT-F displayed reduced σ_{dc}, indicating glycerol and triacetin retard ionic conductivity. YE-F also showed a similar σ_{dc} value as those of YG-F and YT-F. The low σ_{dc} of YE-F could be due to the strong interactions between the IL ions and the charged biopolymers, as discussed above.

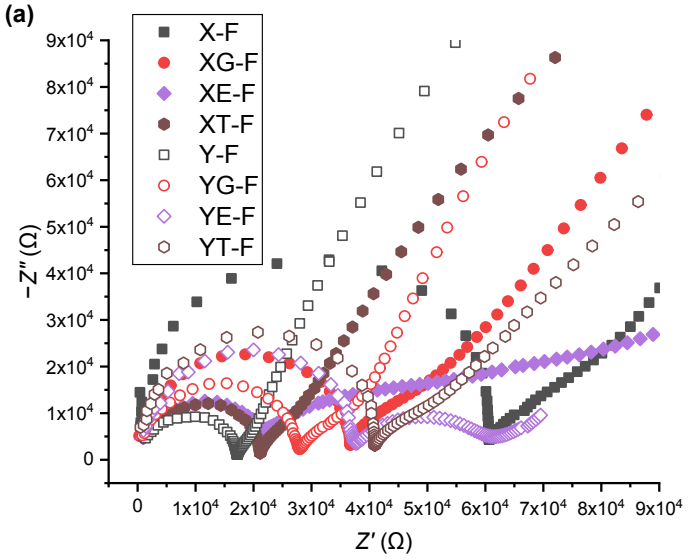

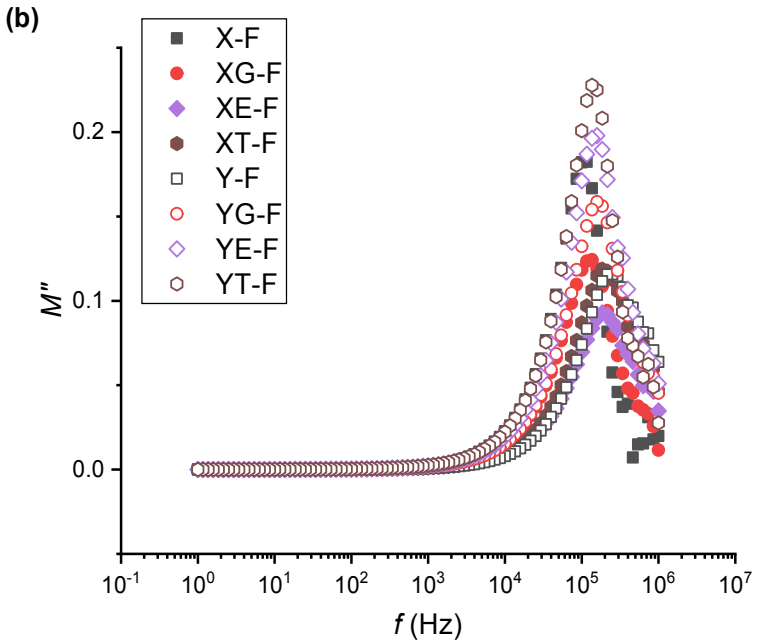

Figure 8. EIS results for the different biopolymer films: a) Nyquist plot of impedance; and b) imaginary electric modulus (M'').

Figure 8 (b) shows for all samples, a well-defined peak for M'' at high f, indicating relaxation processes with a distribution of relaxation times (*i.e.*, viscoelastic relaxation, or dipolar relaxation)[27] For X-F, the peak position was at about 10^5 Hz. In comparison, for the plasticized samples, the peak moved to higher f and became less intense, suggesting a decreased relaxation time. The plasticizer can increase chain mobility and, thus, assist ion and associated dipole mobility. In contrast, compared with Y-F, the plasticized Y-samples displayed a peak shifted to lower f (about 1.3×10^5–1.5×10^5 Hz), indicating a longer relaxation time and decreased mobility of ions and associated dipoles. This trend in relaxation time matches that shown by the σ_{dc} results.

In Summary, our results show that, for the X-matrix, both glycerol and [C_2mim][OAc] were highly effective plasticizers, reducing intra- and intermolecular forces resulting in the chitosan

chains being more mobile and the material more ductile (lower E and σ_t and higher ε_b). The effective plasticization, however, resulted in reduced thermal stability of XG-F and XE-F. XT-F was much more rigid than XG-F and XE-F and even more brittle than X-F. In this regard, triacetin, which is hydrophobic, should have less interaction with chitosan and, thus, a weaker plasticization effect. Interestingly, XRD data shows that the IL assisted the re-crystallization of chitosan but triacetin restricted it, implying the mechanical properties were not in the main determined by crystallinity but the extent of hydrogen bonding. EIS data show that the plasticizers especially the IL increased the mobility of electrical charges in the processed films, thus, increasing their conductivity. Despite its high hydrophilicity, the IL did not significantly reduce surface hydrophilicity. Overall, [C_2mim][OAc] could be considered an excellent plasticizer for chitosan.

For the Y-matrix, plasticization by glycerol or [C_2mim][OAc] also led to reduced thermal stability. STEM images show that chitosan and alginate were not compatible on the sub-micron scale, despite their chemical similarity. Surprisingly, YE-F was the most phase-separated system. Given this, [C_2mim][OAc], as a salt, might disrupt PEC and weaken hydrogen-bonding interactions between chitosan and alginate. As a result, YE-F had distinctly higher surface hydrophilicity than the other samples. The incompatibility between triacetin and the Y-matrix was also apparent in YT-F. Despite the hydrophobicity of triacetin, YT-F displayed the most enhanced re-crystallization of both chitosan and alginate and the highest thermal stability among the Y-series, although being more brittle.

CONCLUSIONS

This work has revealed the strong and unexpected effects of three different plasticizers (*i.e.*, glycerol, [C_2mim][OAc], and triacetin) on the structure (*e.g.*, crystallinity) and properties (*e.g.*, surface hydrophilicity) of chitosan and chitosan/alginate polyelectrolyte complexed materials. The

different effects reflect multiple interactions including hydrogen bonding and ionic forces within such multiphasic systems, whereas the ability of the plasticizer to interrupt hydrogen bonding is not the only determinant factor. The new knowledge obtained from this work can provide insights into the design of plasticized polysaccharide materials with tailored structure and properties.

ASSOCIATED CONTENT

Supporting Information (SI) is available free of charge on the ACS Publications website at DOI: xxx. See SI for supplementary Tables and Figure.

- SEM images (Figure S1), Shore D hardness (Figure S3), electrochemical results (Figure S4 and Table S1) of the different biopolymer films; STEM images of YE-F (Figure S2); and notes to figures

- STEM-HAADF videos showing a "new structure" that was formed under the STEM electron beam and its subsequent changes (Video Clip S1 and Video Clip S2)

AUTHOR INFORMATION

Corresponding Authors

* Fengwei Xie. Email: d.xie.2@warwick.ac.uk, fwhsieh@gmail.com

** Tony McNally. Email: t.mcnally@warwick.ac.uk

Author Contributions

All authors have given approval to the final version of the manuscript. †This author leads the research.

Notes

The authors declare no competing financial interest.

ACKNOWLEDGMENT

The authors acknowledge funding from the European Union's Horizon 2020 research and innovation programme under the Marie Skłodowska-Curie grant agreement No. 798225. P. Chen acknowledges the financial support from the China Scholarship Council (CSC) for her visiting position and thanks IINM, WMG, University of Warwick, UK for hosting her research visit. F. Xie also acknowledges support from the Guangxi Key Laboratory for Polysaccharide Materials and Modification, Guangxi University for Nationalities, China (Grant No. GXPSMM18ZD-02).

ABBREVIATIONS

PEC, polyelectrolyte complexation; RT, room temperature; T_d, thermal decomposition temperature at maximum weight-loss rate; T_β, peak temperature of β-transition; T_α, peak temperature of α-transition; θ_{c0s}, contact angle at 0 s; θ_{c30s}, contact angle at 60 s; θ_{c60s}, contact angle at 60 s

REFERENCES

(1) Xu, W.; Wang, X.; Sandler, N.; Willför, S.; Xu, C. Three-Dimensional Printing of Wood-Derived Biopolymers: A Review Focused on Biomedical Applications. *ACS Sustainable Chem. Eng.* **2018,** *6* (5), 5663–5680.

(2) Chen, J.; Xie, F.; Li, X.; Chen, L. Ionic Liquids for the Preparation of Biopolymer Materials for Drug/Gene Delivery: A Review. *Green Chem.* **2018,** *20* (18), 4169–4200.

(3) Park, S.-B.; Lih, E.; Park, K.-S.; Joung, Y. K.; Han, D. K. Biopolymer-Based Functional Composites for Medical Applications. *Prog. Polym. Sci.* **2017,** *68*, 77–105.

(4) Van Vlierberghe, S.; Dubruel, P.; Schacht, E. Biopolymer-Based Hydrogels as Scaffolds for Tissue Engineering Applications: A Review. *Biomacromolecules* **2011,** *12* (5), 1387–1408.

(5) Lee, A.; Hudson, A. R.; Shiwarski, D. J.; Tashman, J. W.; Hinton, T. J.; Yerneni, S.; Bliley, J. M.; Campbell, P. G.; Feinberg, A. W. 3D Bioprinting of Collagen to Rebuild Components of the Human Heart. *Science* **2019,** *365* (6452), 482–487.

(6) Lin, X.; Liu, Y.; Bai, A.; Cai, H.; Bai, Y.; Jiang, W.; Yang, H.; Wang, X.; Yang, L.; Sun, N.; Gao, H. A Viscoelastic Adhesive Epicardial Patch for Treating Myocardial Infarction. *Nat. Biomed. Eng.* **2019,** *3* (8), 632–643.

(7) Matet, M.; Heuzey, M.-C.; Pollet, E.; Ajji, A.; Avérous, L. Innovative Thermoplastic Chitosan Obtained by Thermo-Mechanical Mixing with Polyol Plasticizers. *Carbohydr. Polym.* **2013,** *95* (1), 241–251.

(8) Gao, C.; Pollet, E.; Avérous, L. Innovative Plasticized Alginate Obtained by Thermo-Mechanical Mixing: Effect of Different Biobased Polyols Systems. *Carbohydr. Polym.* **2017,** *157*, 669–676.

(9) Vieira, M. G. A.; da Silva, M. A.; dos Santos, L. O.; Beppu, M. M. Natural-Based Plasticizers and Biopolymer Films: A review. *Eur. Polym. J.* **2011,** *47* (3), 254–263.

(10) Mekonnen, T.; Mussone, P.; Khalil, H.; Bressler, D. Progress in Bio-Based Plastics and Plasticizing Modifications. *J. Mater. Chem. A* **2013,** *1* (43), 13379–13398.

(11) Tian, H.; Guo, G.; Fu, X.; Yao, Y.; Yuan, L.; Xiang, A. Fabrication, Properties and Applications of Soy-Protein-Based Materials: A Review. *Int. J. Biol. Macromol.* **2018,** *120*, 475–490.

(12) Avérous, L. Biodegradable Multiphase Systems Based on Plasticized Starch: A Review. *Polym. Rev.* **2004,** *44* (3), 231–274.

(13) Šimkovic, I. Unexplored Possibilities of All-Polysaccharide Composites. *Carbohydr. Polym.* **2013,** *95* (2), 697–715.

(14) Shang, S.; Zhu, L.; Fan, J. Intermolecular Interactions Between Natural Polysaccharides and Silk Fibroin Protein. *Carbohydr. Polym.* **2013,** *93* (2), 561–573.

(15) Li, Z.; Ramay, H. R.; Hauch, K. D.; Xiao, D.; Zhang, M. Chitosan–Alginate Hybrid Scaffolds for Bone Tissue Engineering. *Biomaterials* **2005,** *26* (18), 3919–3928.

(16) Wei, C.; Zhu, X.; Peng, H.; Chen, J.; Zhang, F.; Zhao, Q. Facile Preparation of Lignin-Based Underwater Adhesives with Improved Performances. *ACS Sustainable Chem. Eng.* **2019,** *7* (4), 4508–4514.

(17) Meng, L.; Xie, F.; Zhang, B.; Wang, D. K.; Yu, L. Natural Biopolymer Alloys with Superior Mechanical Properties. *ACS Sustainable Chem. Eng.* **2019,** *7* (2), 2792–2802.

(18) Basu, S.; Plucinski, A.; Catchmark, J. M. Sustainable Barrier Materials Based on Polysaccharide Polyelectrolyte Complexes. *Green Chem.* **2017,** *19* (17), 4080–4092.

(19) Chen, P.; Xie, F.; Tang, F.; McNally, T. Thermomechanical-Induced Polyelectrolyte Complexation between Chitosan and Carboxymethyl Cellulose Enabling Unexpected Hydrolytic Stability. *Compos. Sci. Technol.* **2020,** *189*, 108031.

(20) Iwasaki, N.; Yamane, S.-T.; Majima, T.; Kasahara, Y.; Minami, A.; Harada, K.; Nonaka, S.; Maekawa, N.; Tamura, H.; Tokura, S.; Shiono, M.; Monde, K.; Nishimura, S.-I. Feasibility of Polysaccharide Hybrid Materials for Scaffolds in Cartilage Tissue Engineering: Evaluation of Chondrocyte Adhesion to Polyion Complex Fibers Prepared from Alginate and Chitosan. *Biomacromolecules* **2004,** *5* (3), 828–833.

(21) Murakawa, K.; King, D. R.; Sun, T.; Guo, H.; Kurokawa, T.; Gong, J. P. Polyelectrolyte Complexation via Viscoelastic Phase Separation Results in Tough and Self-Recovering Porous Hydrogels. *J. Mater. Chem. A* **2019,** *7* (35), 5296–5305.

(22) Tian, H.; Guo, G.; Xiang, A.; Zhong, W.-H. Intermolecular Interactions and Microstructure of Glycerol-Plasticized Soy Protein Materials at Molecular and Nanometer Levels. *Polym. Test.* **2018,** *67*, 197–204.

(23) Ren, F.; Wang, J.; Xie, F.; Zan, K.; Wang, S.; Wang, S. Applications of Ionic Liquids in Starch Chemistry: A Review. *Green Chem.* **2020,** *22* (7), 2162–2183.

(24) Osman, Z.; Ibrahim, Z. A.; Arof, A. K. Conductivity Enhancement due to Ion Dissociation in Plasticized Chitosan Based Polymer Electrolytes. *Carbohydr. Polym.* **2001,** *44* (2), 167–173.

(25) Bhatt, A. S.; Bhat, D. K.; Santosh, M. S.; Tai, C.-w. Chitosan/NiO Nanocomposites: A Potential New Dielectric Material. *J. Mater. Chem.* **2011,** *21* (35), 13490–13497.

(26) Bowen Chris, R.; Buschhorn, S.; Adamaki, V. Manufacture and Characterization of Conductor-Insulator composites Based on Carbon Nanotubes and Thermally Reduced Graphene Oxide. *Pure Appl. Chem.* **2014,** *86* (5), 765–774.

(27) Fadzallah, I. A.; Majid, S. R.; Careem, M. A.; Arof, A. K. Relaxation Process in Chitosan–Oxalic Acid Solid Polymer Electrolytes. *Ionics* **2014,** *20* (7), 969–975.

(28) Palma, F.; Michniak-Kohn, B.; Pérez-Correa, J. R.; Hernandez, E.; Romañach, R. J.; Valenzuela, L. M. Near-Infrared Chemical Imaging and Its Correlation with the Mechanical Properties of Chitosan–Gelatin Edible Films. *Carbohydr. Polym.* **2016,** *136*, 409–417.

(29) Morris, E. R.; Rees, D. A.; Thom, D.; Boyd, J. Chiroptical and Stoichiometric Evidence of a Specific, Primary Dimerisation Process in Alginate Gelation. *Carbohydr. Res.* **1978,** *66* (1), 145–154.

(30) Li, L.; Fang, Y.; Vreeker, R.; Appelqvist, I.; Mendes, E. Reexamining the Egg-Box Model in Calcium−Alginate Gels with X-Ray Diffraction. *Biomacromolecules* **2007,** *8* (2), 464–468.

(31) Sikorski, P.; Mo, F.; Skjåk-Bræk, G.; Stokke, B. T. Evidence for Egg-Box-Compatible Interactions in Calcium−Alginate Gels from Fiber X-Ray Diffraction. *Biomacromolecules* **2007,** *8* (7), 2098–2103.

(32) Lawrie, G.; Keen, I.; Drew, B.; Chandler-Temple, A.; Rintoul, L.; Fredericks, P.; Grøndahl, L. Interactions Between Alginate and Chitosan Biopolymers Characterized Using FTIR and XPS. *Biomacromolecules* **2007,** *8* (8), 2533–2541.

(33) Pawlak, A.; Mucha, M. Thermogravimetric and FTIR Studies of Chitosan Blends. *Thermochim. Acta* **2003,** *396* (1–2), 153–166.

(34) Chen, Z.; Mo, X.; He, C.; Wang, H. Intermolecular Interactions in Electrospun Collagen–Chitosan Complex Nanofibers. *Carbohydr. Polym.* **2008,** *72* (3), 410–418.

(35) Papageorgiou, S. K.; Kouvelos, E. P.; Favvas, E. P.; Sapalidis, A. A.; Romanos, G. E.; Katsaros, F. K. Metal–Carboxylate Interactions in Metal–Alginate Complexes Studied with FTIR Spectroscopy. *Carbohydr. Res.* **2010,** *345* (4), 469–473.

(36) Kittur, F. S.; Vishu Kumar, A. B.; Tharanathan, R. N. Low Molecular Weight Chitosans—Preparation by Depolymerization with *Aspergillus Niger* Pectinase, and Characterization. *Carbohydr. Res.* **2003,** *338* (12), 1283–1290.

(37) Dou, B.; Dupont, V.; Williams, P. T.; Chen, H.; Ding, Y. Thermogravimetric Kinetics of Crude Glycerol. *Bioresour. Technol.* **2009,** *100* (9), 2613–2620.

(38) Wendler, F.; Todi, L.-N.; Meister, F. Thermostability of Imidazolium Ionic Liquids as Direct Solvents for Cellulose. *Thermochim. Acta* **2012,** *528*, 76–84.

(39) Quijada-Garrido, I.; Laterza, B.; Mazón-Arechederra, J. M.; Barrales-Rienda, J. M. Characteristic Features of Chitosan/Glycerol Blends Dynamics. *Macromol. Chem. Phys.* **2006,** *207* (19), 1742–1751.

(40) Quijada-Garrido, I.; Iglesias-González, V.; Mazón-Arechederra, J. M.; Barrales-Rienda, J. M. The Role Played by the Interactions of Small Molecules with Chitosan and Their Transition Temperatures. Glass-Forming Liquids: 1,2,3-Propantriol (Glycerol). *Carbohydr. Polym.* **2007,** *68* (1), 173–186.

(41) Bonanos, N.; Steele, B. C. H.; Butler, E. P. Applications of Impedance Spectroscopy. In *Impedance Spectroscopy*; Barsoukov, E.; Macdonald, J. R., Eds.; John Wiley & Sons, Inc.: Hoboken, NJ, USA, 2005; Chapter 4, pp 205–537.

- Table of Contents -

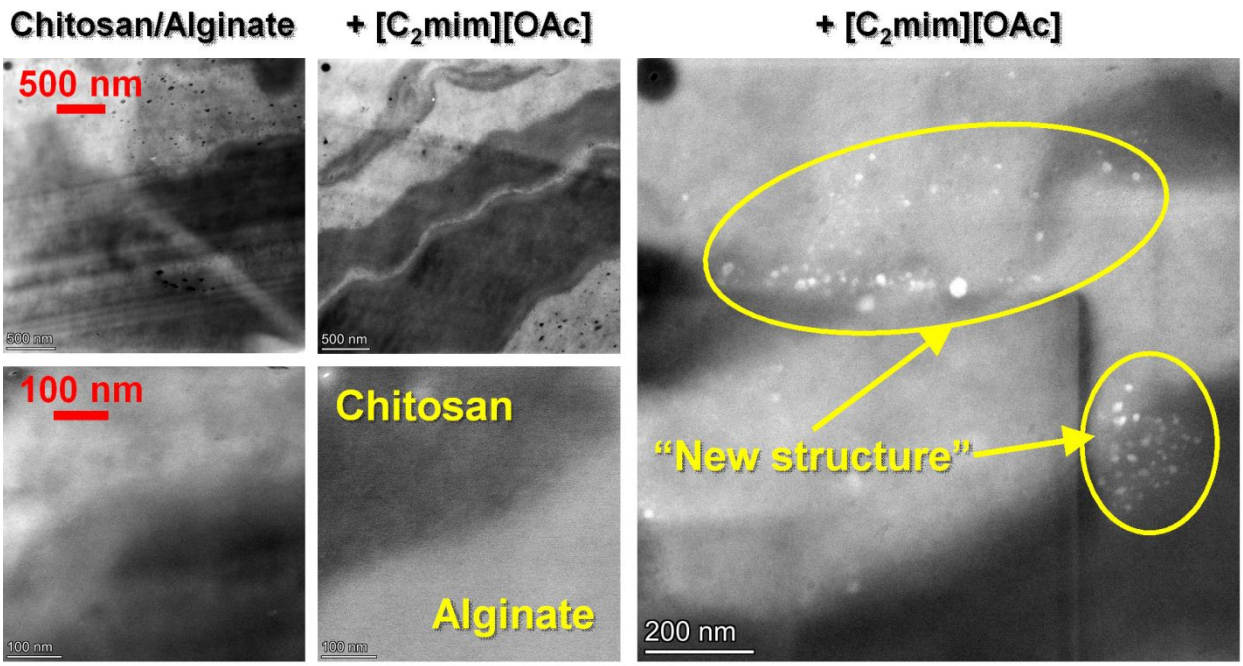

SYNOPSIS

1-Ethyl-3-methylimidazolium acetate has strong and unexpected effects on the hydrogen bonding and electrostatic interactions within chitosan/alginate polyelectrolyte complexed materials.

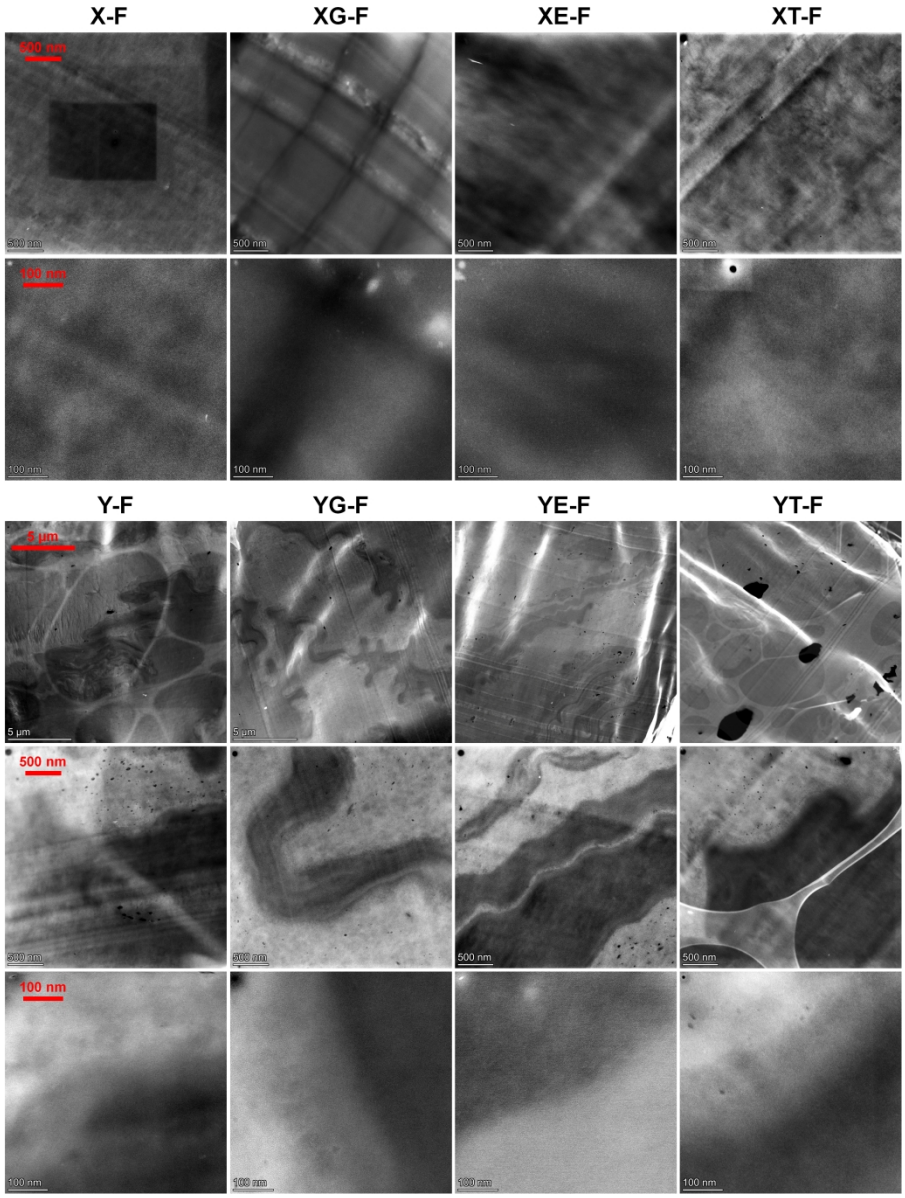

Figure 1. STEM-HAADF images of the different biopolymer films.

675x901mm (144 x 144 DPI)

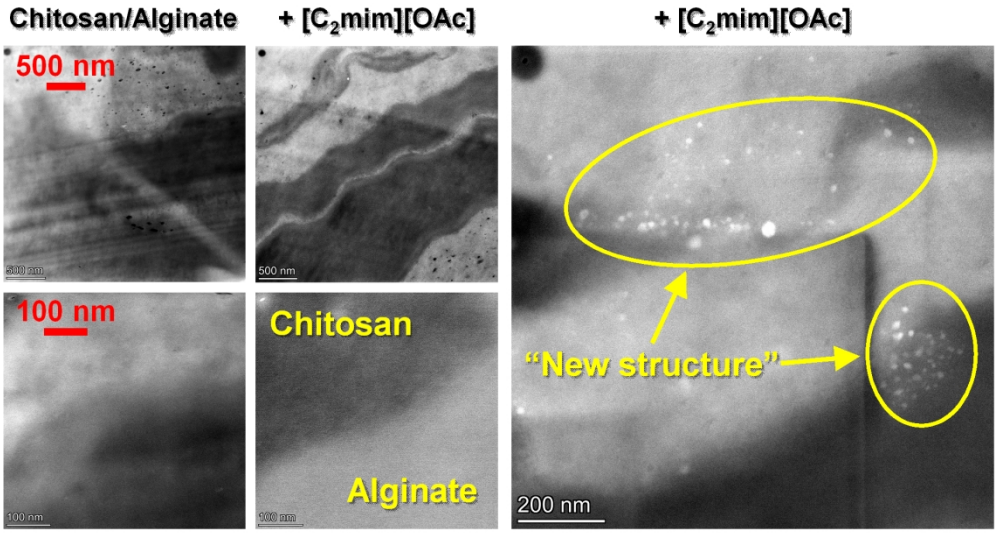

Table of Content Graphic

352x198mm (144 x 144 DPI)